

Article

Monitoring the Landscape Pattern Dynamics and Driving Forces in Dongting Lake Wetland in China Based on Landsat Images

Mengshen Guo ¹, Nianqing Zhou ^{1,*}, Yi Cai ¹, Wengang Zhao ², Shuaishuai Lu ¹ and Kehao Liu ¹

¹ College of Civil Engineering, Tongji University, Shanghai 200092, China; masion_kwok@163.com (M.G.); caiyi@tongji.edu.cn (Y.C.); lushuaishuai@tongji.edu.cn (S.L.); 2232626@tongji.edu.cn (K.L.)

² Hunan Institute of Water Resources and Hydropower Research, Changsha 410007, China; zwg921153@163.com

* Correspondence: nq.zhou@tongji.edu.cn

Abstract: Dongting Lake wetland is a typical lake wetland in the Middle and Lower Yangtze River Plain in China. Due to the influence of natural and human activities, the landscape pattern has changed significantly. This study used 12 Landsat images from 1991 to 2022 and applied three common classification methods (support vector machine, maximum likelihood, and CART decision tree) to extract and classify the landscape information, with the latter having a superior annual accuracy of over 90%. Based on the CART decision tree classification results, the dynamic characteristics of wetland spatial patterns were analyzed through the landscape pattern index, dynamic degree model, and transition matrix model. Redundancy and grey correlation analysis were employed to investigate the driving factors. The results showed increased landscape fragmentation, reduced heterogeneity, and increased complexity from 1991 to 2022. The water and mudflat areas exhibited three distinct stages: gradual decline until 2001 ($-3.06 \text{ km}^2/\text{a}$); sharp decrease until 2014 ($-19.44 \text{ km}^2/\text{a}$); and steady increase ($22.93 \text{ km}^2/\text{a}$). Vegetation conversion, particularly between sedge and reed, dominated the change in landscape pattern. Reed area initially increased ($18.88 \text{ km}^2/\text{a}$), then decreased ($-35.89 \text{ km}^2/\text{a}$), while sedge showed the opposite trend. Woodland area fluctuated, peaking in 2016 and declined by 2022. The construction of the Three Gorges Dam significantly altered landscape dynamics through water level changes, reflected by a 4.03% comprehensive dynamic degree during 2001–2004. Potential evaporation also emerged as a significant natural factor, exhibiting a negative correlation with the landscape index. During 1991–2001 and 2004–2022, the comprehensive explanatory rates of temperature, precipitation, potential evaporation, and water level on landscape pattern dynamics were 88.56% and 52.44%, respectively. Other factors like policies and socio-economic factors played a crucial role in wetland change. These findings offer valuable insights into the dynamic evolution and driving mechanisms of Dongting Lake wetland.

Keywords: wetland change; landscape pattern; CART decision tree model; driving forces; Dongting Lake



Citation: Guo, M.; Zhou, N.; Cai, Y.; Zhao, W.; Lu, S.; Liu, K. Monitoring the Landscape Pattern Dynamics and Driving Forces in Dongting Lake Wetland in China Based on Landsat Images. *Water* **2024**, *16*, 1273. <https://doi.org/10.3390/w16091273>

Academic Editor: Richard Smardon

Received: 22 March 2024

Revised: 23 April 2024

Accepted: 26 April 2024

Published: 29 April 2024



Copyright: © 2024 by the authors. Licensee MDPI, Basel, Switzerland. This article is an open access article distributed under the terms and conditions of the Creative Commons Attribution (CC BY) license (<https://creativecommons.org/licenses/by/4.0/>).

1. Introduction

Wetlands are a natural complex formed by the interaction between water and land [1], which are one of the ecosystems with the highest biological productivity and economic value in the world [2], ranking alongside forest and marine ecosystems as the three major ecosystems on Earth. They have unique ecological and hydrological environmental conditions [3], playing an important role in regulating floods, improving water quality, regulating climate, and maintaining regional ecological balance, and are known as the “kidney of the Earth” [4,5]. However, due to the dual impact of natural and human activities, the global wetlands ecosystem has been damaged or degraded directly or indirectly [6], which not only has various adverse effects on wetland water resources, water environment, water ecology, and biodiversity but also have important constraints on sustainable socio-economic development [7,8]. With the rise in global temperature and the frequent occurrence of

various extreme climate events, “Carbon Peak” and “Carbon Neutrality” have become a hot topic of concern at home and abroad in recent years. Wetlands have the functions of “carbon source” and “carbon sink” [9]. Increasing the area of wetlands, enhancing the service function of existing wetland ecosystems, and increasing wetland carbon absorption through ecological carbon sequestration can play a positive role in achieving “Carbon Neutrality”. Therefore, strengthening wetland monitoring, understanding wetland landscape pattern change, and wetland functional decline degree have become key to wetland protection and restoration.

Due to the long-term dynamic process of wetland evolution, remote sensing technology has been widely used in wetland ecological evaluation, wetland dynamic monitoring, and wetland landscape pattern analysis in the past 30 years [10–12]. Remote sensing technology originated from agricultural geographical monitoring in developed countries in Europe and the United States in the 1990s. It has the advantages of being easy to obtain, multi-temporal and multi-resolution, and can conduct extensive and long-term observations. With the development of computer science and the continuous accumulation of remote sensing image data, including NOAAAVHRR, Landsat MSS/TM/ETM+, and SPOT, wetland research techniques have also shifted from a single qualitative evaluation to quantitative research based on 3S technology and models [4,13,14]. Ahmadzadeh et al. [15] utilized Landsat 5, 7, and 8 satellite imagery and the Carlson Trophic State Index (TSI) to monitor and analyze the impact of trophic processes on landscape structural changes and assessed changes in wetland vegetation canopy and water bodies in Anzali Wetland from 1994 to 2018. Fan et al. [16] examined wetland phenology from 30 m harmonized Landsat/Sentinel-2 (LandSent30) and 500 m MODIS satellite observations using the ground phenology network as a benchmark, highlighting LandSent30's better alignment with PhenoCam data. Zhang and Lin [17] used an ensemble method combining Sentinel-1 SAR time series and segmentations generated from GF-6 MPS images to obtain an accurate wetland map for the Dongting Lake wetlands in China, achieving higher classification accuracy compared to pixel-based methods. Cheng et al. [18] employed a Support Vector Machine to conduct a supervised classification of ZY1-02D satellite hyperspectral remote sensing images in the Yellow River Estuary and utilized a Random Forest model to predict landscape diversity using spectral diversity. The extraction of wetland information has been substantially improved, providing a scientific decision-making basis for wetland resource protection and restoration.

Lake wetlands are distributed all over the world, directly exposed to various geophysical environments, and are highly sensitive to climate change. In densely populated areas, they are also subject to additional impacts from human activities related to diversion and consumption [19,20]. Dongting Lake wetland in the middle reaches of the Yangtze River in China is a typical freshwater wetland with siltation worldwide. Due to the construction of the Three Gorges Dam and the reclamation of the lake for farmland, the relationship between Dongting Lake and the Yangtze River has undergone multiple adjustments [21], forming a complex hydrological environment and wetland structure involving the lake wetland ecosystem, lake-river interactions, and human geography due to its seasonal floods, periodic rapid replacement of lake water, and close hydrological connectivity with major rivers. Numerous studies have primarily concentrated on qualitative descriptions and statistical analysis of Dongting Lake, particularly regarding the impact of the Three Gorges Dam operation on wetland changes. Peng et al. [22] utilized a multi-spectral index method based on decision tree classification to assess surface water changes and their driving factors in Dongting Lake. Ye [23] studied land-type data mining in high-resolution remote sensing images of the Dongting Lake area using the QUEST decision tree, highlighting the enhancement in classification accuracy with multi-scale texture features. Liu et al. [11] applied the CART method to delineate the wetland area in the middle reaches of the Yangtze River and conducted a quantitative evaluation of wetland health based on the PSR model from 2000 to 2019. Hu et al. [24] used multi-temporal remote sensing images to investigate the influence of hydrological changes on vegetation distribution in

Dongting Lake and analyzed the disparities before and after the implementation of the Three Gorges Dam. However, studies using higher-resolution images to reveal the overall changes in Dongting Lake wetland are limited, often confined to specific areas rather than the entire region.

This study aims to analyze the long-term landscape changes in the entire Dongting Lake wetland using medium-resolution images. Landsat TM/ETM+/OLI images were utilized, and an appropriate classification method was selected from those applicable to medium-resolution imagery, including Support Vector Machine (SVM), Maximum Likelihood (ML), and Decision Tree (DT), to extract vegetation information from the Dongting Lake wetland. From 1991 to 2022, the spatiotemporal variations in wetland patterns were characterized using landscape pattern indices, dynamic degree models, and transition matrix models. Redundancy Analysis (RDA) and Grey Relational Analysis (GRA) were employed to explore the response of wetland landscape evolution to climate and human activities. It provides some reference value for monitoring and managing wetlands amidst natural and social challenges.

2. Materials and Methods

2.1. Study Area

Dongting Lake ($28^{\circ}30' N \sim 30^{\circ}20' N$, $111^{\circ}40' E \sim 113^{\circ}10' E$) is located in the northeast of Hunan Province, on the south bank of the Jingjiang River in the middle reaches of the Yangtze River. It is the second largest freshwater lake in China and consists of East Lake, South Lake, and West Lake (Muping Lake and Qili Lake), with the reputation of being the “kidney of the Yangtze River” [25]. There are seven water inlets feeding Dongting Lake, including four rivers (Xiangjiang River, Zishui River, Yuanjiang River, and Lishui River) and three outlets (Songzi River, Taiping River, and Ouchi River). After sedimentation and purification, the water flows out of Chenglingji Hydrological Station and into the Yangtze River [26]. Generally speaking, Dongting Lake is the most complex water system region in the world. The study area was within the planning boundary of the Dongting Lake wetland Protection Zone (Figure 1), with a total area of approximately 2680.29 km².

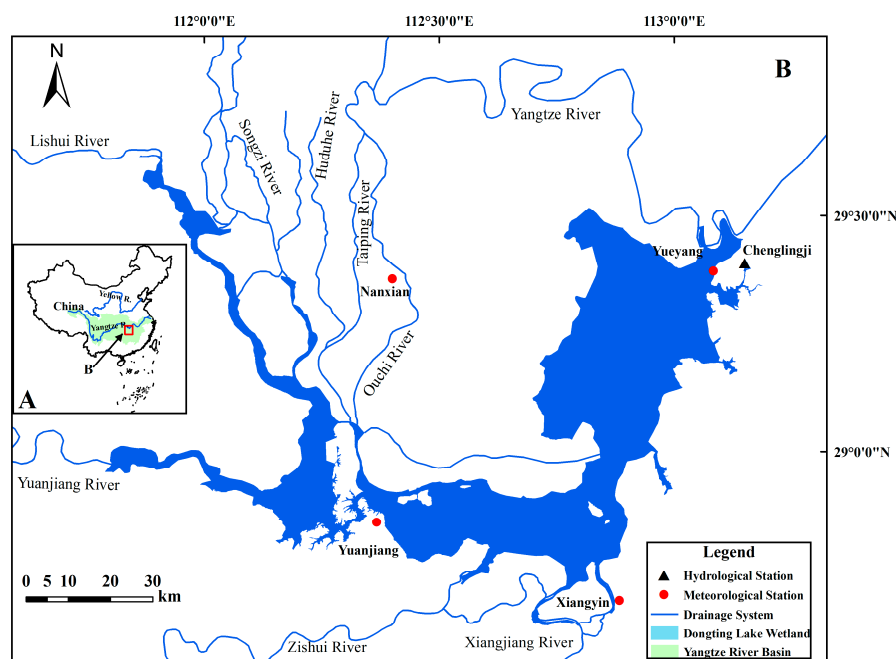


Figure 1. Location of Dongting Lake wetland.

Dongting Lake wetland is a subtropical humid monsoon climate with four distinct seasons, abundant heat, and precipitation. The average annual temperature is 16.15 °C, and the annual precipitation is 1148~1837 mm [27]. Affected by seasonal variations in the

watershed and the inflow of the Yangtze River, the water level fluctuates significantly, with an average water level of 25 m over the years and an annual variation of about 12.5 m. Long-term seasonal flooding has resulted in a complex landscape feature of shallow water, mudflat, and vegetation, with different plants occupying specific ecological niches on the beach.

2.2. Datasets and Pre-Processing

2.2.1. Remote Sensing Data

In this study, we selected 12 periods of Landsat TM/ETM+/OLI (spatial resolution of 30 m) images from USGS (<https://earthexplorer.usgs.gov/>, accessed on 23 July 2023) with cloud cover <30% from 1991 to 2022, totaling 24 scenes. The track number and specific acquisition time are shown in Table 1. Considering that most Dongting Lake beaches were exposed in autumn and winter, and the reed began to wither and harvest, it is easy to distinguish from the sedge in the image. Additionally, this period represents the late stage of vegetation growth with relatively stable conditions, which can ensure the inter-annual comparability of wetland vegetation [28]. Thus, the image acquisition time was between October and December.

Table 1. The type and time of Landsat images.

Number	Year	Row/Path: 123/40		Row/Path: 124/40		Water Level (m)
		Data	Satellite	Data	Satellite	
1	1991	11.8	TM	11.15	TM	22.96
2	1993	12.31	TM	12.6	TM	22.43
3	1995	12.5	TM	12.28	TM	20.77
4	1999	12.24	ETM+	12.15	ETM+	21.30
5	2001	12.29	ETM+	10.1	ETM+	20.56
6	2004	12.5	ETM+	12.12	ETM+	22.19
7	2008	12.8	TM	12.31	TM	21.64
8	2010	11.12	TM	11.19	TM	21.88
9	2014	12.17	ETM+	12.8	ETM+	22.65
10	2016	11.28	OLI	12.5	OLI	21.87
11	2020	11.7	OLI	11.14	OLI	23.80
12	2022	12.23	OLI	12.22	OLI	19.44

Before extracting wetland landscape information, a series of processing was carried out on remote sensing images, mainly including radiometric calibration, FLAASH atmospheric correction, geometric correction, spectral enhancement, optimal band selection, image mosaic, and cropping. These procedures were implemented based on the ENVI 5.6 software. We opted for the 543-band combination to interpret from 1990 to 2014 and the 654-band combination from 2016 to 2022 since there are characteristic differences in the Landsat 8 OLI, Landsat 5 TM, and Landsat 7 ETM+ bands. Notably, owing to machine malfunctions in the Landsat 7 ETM+ images, there was a loss of stripes in images obtained after 2003. To address this issue, we used the extension tool Landsat_gapfill for image restoration [29].

2.2.2. Field Measurement Data

Field investigations were conducted on the distribution and structure of vegetation in Dongting Lake wetland between December 2022 and January 2023. The survey site covered a total of 8 wetland beaches in the East Lake, West Lake, and South Lake Reserve. Detailed geographic coordinates and community names of each wetland type were recorded using GPS, resulting in nearly 220 coordinate information points. Beaches that could not be located on site were photographed and marked in detail on the map. We randomly selected 182 points of information combined with images as a region of interest (ROI) for remote sensing image interpretation and extraction; the other 38 points of information were used for classification accuracy verification.

2.2.3. Hydrology and Meteorological Data

The hydrological data were obtained from the monthly water level observation data of Chenglingji Hydrological Station in Dongting Lake from 1991 to 2022, sourced from the “Hydrological Data of the Yangtze River Basin” (<http://www.cjw.gov.cn/zwzc/zjgb/>, accessed on 15 August 2023). Daily ground climate data in Hunan Province were obtained from the National Meteorological Data Center (<http://data.cma.cn>, accessed on 10 August 2023). We chose daily precipitation and average temperature data from Yueyang, Xiangyin, Yuanjiang, and Nanxian meteorological stations within the Dongting Lake wetland area from 1991 to 2022 (Figure 1).

Potential evapotranspiration (ET_p) is an indispensable process in the atmospheric, hydrosphere, and biosphere cycles. ET_p , together with precipitation, determines the arid and humid states of the region, which can be calculated according to the Penman–Monteith formula [30]. This formula is based on the principles of energy balance and water vapor turbulent diffusion and comprehensively considers the impact of meteorological factors such as temperature, sunshine duration, relative humidity, and wind speed on evapotranspiration, which is widely used to estimate potential evapotranspiration at different regional scales [31]. It is expressed as follows:

$$ET_p = \frac{0.408D(R_n - G) + \frac{900}{T+273}u_2(e_s - e_a)}{D + g(1 + 0.34u_2)} \quad (1)$$

where ET_p is the potential evaporation (mm); D is the slope of the saturated water vapor pressure curve ($Kpa \cdot ^\circ C^{-1}$); R_n is the net radiation ($MJ \cdot m^{-2} \cdot d^{-1}$); G is the soil heat flux ($MJ \cdot m^{-2} \cdot d^{-1}$); g is the psychrometric constant ($Kpa \cdot ^\circ C^{-1}$); T is the average temperature at 2 m ($^\circ C$); u_2 is the average wind speed at 2 m height ($m \cdot s^{-1}$); e_s is the saturated water vapor pressure (Kpa); e_a is the actual water vapor pressure (KPa). In this paper, the ET_0 Calculator software (<http://www.fao.org/land-water/databases-and-software/eto-calculator/en/>, accessed on 12 August 2023) was used to calculate the daily potential evaporation of Dongting Lake wetland from 1991 to 2022.

To eliminate the impact of the one-sidedness of the location of meteorological stations, the monthly average temperature, precipitation, and potential evaporation of Dongting Lake wetland were given different weights based on the contribution of each station to the overall monthly averages of all four stations.

2.3. Methodology

Three commonly used medium-resolution imagery classification methods (SVM, ML, and DT) based on pixels and pixel spectral characteristics were employed to divide the Dongting Lake wetland landscape from 1991 to 2022 into five categories, including water, mudflat, sedge, reed, and woodland. In this paper, the DT method utilized the CART decision tree method, as detailed in Section 2.3.1. Descriptions and applications of the SVM and the ML method can be found in other references [32,33]. This classification was based on ROI derived from field measurement data combined with visual interpretation. Subsequently, the confusion matrix was used to evaluate the accuracy of the image, with the optimal classification method chosen based on accuracy and the Kappa coefficient for subsequent wetland landscape pattern analysis. The whole operation was conducted using ENVI 5.6 software. The landscape pattern analysis indicator system corresponds to patch, class, and landscape levels [34]. We selected the landscape-level index and employed Fragstats 4.2 software to analyze wetland landscape patterns. Moreover, the wetland landscape dynamism and the transition matrix between wetland landscape types were analyzed using dynamic degree models and transition matrix models within ArcGIS 10.8 software. To explain the dynamics of wetland landscape pattern, the contribution rates of human activities (quantified by water level [H], reflecting the water level in the Dongting Lake area and Chenglingji Hydrological Station at the exit, considered a social factor) and climate change (represented by temperature [T], precipitation [P] and potential evaporation

[ET_p]) were quantitatively calculated using RDA and GRA via CANOCO 5.0 software and SPSSAU (<https://spssau.com/index.html>, accessed on 3 September 2023), respectively. A technical flowchart of the analysis is shown in Figure 2.

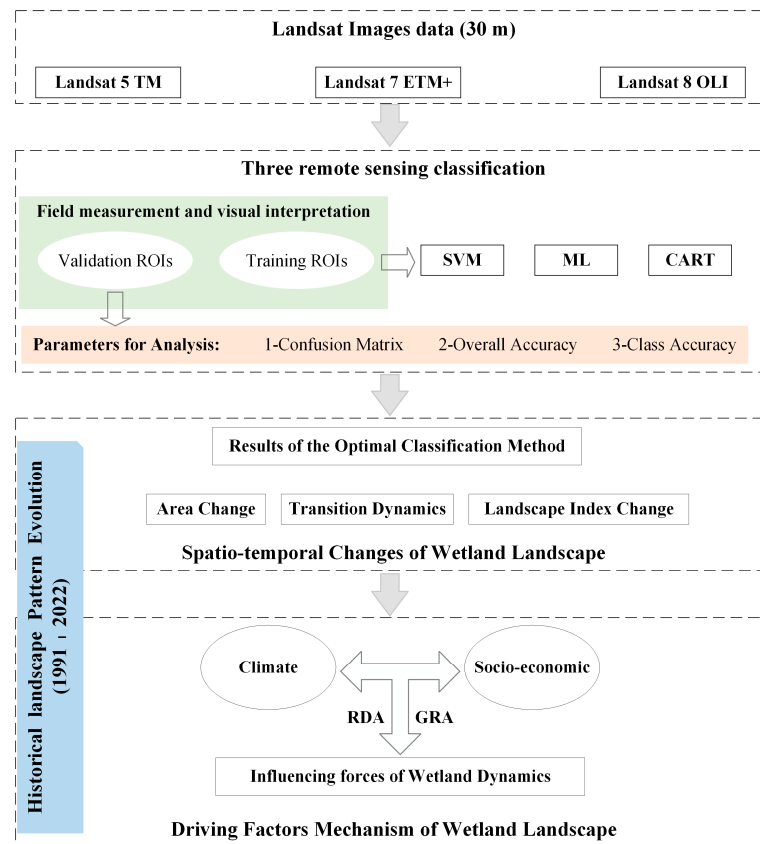


Figure 2. Flow chart of landscape pattern dynamics and driving forces analysis in Dongting Lake wetland based on Landsat images.

2.3.1. CART Decision Tree Classification Method

The CART method is a nonlinear, non-parametric data mining and classification prediction method with accurate and reliable prediction models. It constructs a binary tree to perform classification by recursively partitioning the training dataset composed of input and output variables [35]. During the tree growth, the reduction in the Gini coefficient is used as a criterion to select the attribute that maximizes the reduction, thus determining the optimal variable to group the training set and establish a binary decision tree. Its mathematical definition is as follows:

$$G(t) = 1 - \sum_{j=1}^k P^2(j|t) \quad (2)$$

where $G(t)$ is the Gini coefficient; t is the node; k is the number of categories of output variables; $P(j|t)$ is the normalized probability of taking j as the sample output variable in the node. Supposing that the sample dataset N is divided into two groups using the feature attribute M , the Gini coefficient is

$$G(t) = \frac{N_1}{N}G(t_1) + \frac{N_2}{N}G(t_2) \quad (3)$$

thus, the Gini coefficient after grouping decreased by

$$\Delta G(t) = G(t) - \left[\frac{N_1}{N}G(t_1) + \frac{N_2}{N}G(t_2) \right] \quad (4)$$

where $G(t)$ and N are the Gini coefficient and sample size of the output variables before grouping, respectively. $G(t_1)$, N_1 and $G(t_2)$, N_2 are the Gini coefficients and sample sizes of the right and left subtrees after grouping. The optimal split point for grouping variables is reached when the total heterogeneity of the two sets of output variable values is minimized, resulting in the sample category variables tending to have the same category values after grouping, thereby maximizing purity. This process continues until the decision tree classification is completed.

2.3.2. Landscape Pattern Index

This study selected six landscape indices, including two landscape fragmentation indices (patch density [PD] and edge density [ED]), two landscape diversity indices (Shannon diversity index [SHDI] and Shannon evenness index [SHEI]), two landscape heterogeneity indices (landscape shape index [LSI], and average fractal dimension [FRAC_MN]) [36].

1. PD

PD refers to the number of patches per unit area in a landscape, including all heterogeneous landscape elements and can be used to characterize the degree of fragmentation. The higher the value, the higher the landscape fragmentation degree. The formula is as follows:

$$PD = \frac{\sum_{i=1}^n M_i}{A} \quad (5)$$

where n is the total number of landscape types; M_i is the number of patches in the i -th type of landscape; A is the total area of the landscape.

2. ED

ED refers to the edge length between heterogeneous landscape patches per unit area, revealing the degree a landscape is fragmented by boundaries. It is a direct reflection of the degree of landscape fragmentation. The higher the value, the more heterogeneous landscape patches, and the more fragmented the landscape. The formula is as follows:

$$ED = \frac{1}{X} \int_{i=1}^Y \int_{j=1}^Y P_{ij} \quad (6)$$

where P_{ij} is the boundary length between the i -th type landscape patch and the adjacent j -th type landscape patch.

3. SHDI

SHDI can accurately identify the spatial uneven distribution of various patch types in the landscape. The larger the value, the more heterogeneous patches in the landscape pattern and the more fragmented the landscape. The formula is as follows:

$$SHDI = - \sum_{i=1}^n (P_i \ln P_i), SHDI \geq 0 \quad (7)$$

where P_i is the proportion of the i -type landscape to the total landscape.

4. SHEI

SHEI can reflect the evenness of landscape-type distribution. $SHEI = 0$ indicates that the landscape consists of only one patch type without diversity; $SHEI = 1$ indicates that the class types are evenly distributed with maximum diversity and highest uniformity. Therefore, the larger the value, the more evenly distributed the class types in the landscape, and there is no obvious advantage class. The formula is as follows:

$$SHEI = \frac{-\sum_{i=1}^n (P_i \ln P_i)}{\ln n}, 0 \leq SHEI \leq 1 \quad (8)$$

5. LSI

LSI reflects the regularity of landscape patches and the complexity of edges. Generally speaking, the larger the value, the more complex the shape of the landscape patch and the higher the degree of landscape fragmentation. The formula is as follows:

$$LSI = \frac{0.25 \int_i^n e_{ji}}{\sqrt{\pi A}} \quad (9)$$

where e_{ji} is the total edge length between the i -type landscape patch and the j -type landscape patch.

6. FRAC_MN

FRAC_MN describes the complexity of patches based on patch area, summarizing the landscape as the average fractal dimension index of all patches. The formula is as follows:

$$FRAC_MN = \frac{FRAC[patch_{ij}]}{n} \quad (10)$$

where $FRAC[patch_{ij}]$ is the fractal dimension index of each patch. If all patches are square, $FRAC_MN = 1$; if all patches are irregular, then $FRAC_MN$ is close to 2.

2.3.3. Dynamic Degree and Transition Matrix Models

7. Dynamic degree model

The dynamic degree model calculates the landscape dynamic changes, with formulas for single and comprehensive landscapes as follows:

$$DC = \frac{U_b - U_a}{U_a} \times \frac{1}{T} \times 100\% \quad (11)$$

$$L_c = \frac{\sum_{i=1}^n \Delta L_{U_{i-j}}}{2 \sum_{i=1}^n \Delta L_{U_i}} \times \frac{1}{T} \times 100\% \quad (12)$$

where DC is the dynamic degree of single wetland landscape change during the study period, %; L_c is the comprehensive wetland landscape dynamics change, %; U_a , U_b are, respectively, the wetland landscape area at the beginning and end of the study period, km^2 ; $\Delta L_{U_{i-j}}$ is the absolute value of the area, where the i -type landscape transforms into a non- i -type landscape; ΔL_{U_i} is the area of the previous landscape type, km^2 ; T is the study period, a.

8. Transition matrix model

By analyzing the landscape type transition matrix, the mutual transformation status between various landscape types can be quantitatively explained, and the transition rate between different landscape types can be revealed, providing a better understanding of the landscape dynamics process. The expression of the transition matrix is as follows:

$$S_{ij} = \begin{vmatrix} S_{11} & \cdots & S_{1n} \\ \cdots & \cdots & \cdots \\ S_{n1} & \cdots & S_{nn} \end{vmatrix} \quad (13)$$

where n is the number of wetland landscape types; i , j are the landscape types at the beginning and end of the period, respectively; S_{ij} is the area transferred from the i -type landscape to the j -type landscape during the study period, km^2 .

3. Results

3.1. Accuracy Verification Results of SVM, ML, and CART Methods

A total of 91 ROIs were selected for verification based on 38 measured points combined with remote-sensing images. Table 2 illustrates that the average classification accuracy using the CART algorithm is 92.80%, with a Kappa coefficient of 0.9074 from 1991 to 2022. A comparison revealed that the SVM method achieved an accuracy of 93.26%, with a Kappa coefficient of 0.9130, and the ML method reached a 92.38% accuracy, with a Kappa coefficient of 0.9024. Despite the similar trends observed in the three commonly used classification methods for medium-resolution images, the CART decision tree consistently maintained an annual classification accuracy exceeding 90%. Conversely, the SVM method attained accuracies of 88.29% and 86.76% in 1993 and 2022, respectively, and the ML algorithm resulted in accuracies of 89.20% and 76.91% in 2016 and 2022, respectively, all falling below 90%. Thus, the CART decision tree demonstrated superior applicability in Dongting Lake wetland.

Table 2. Classification accuracy verification results of SVM, ML, and CART methods.

Year	SVM		ML		CART	
	Accuracy	Kappa	Accuracy	Kappa	Accuracy	Kappa
1991	93.59%	0.9171	92.43%	0.9029	93.09%	0.9111
1993	88.29%	0.8470	92.47%	0.9012	90.80%	0.8794
1995	94.68%	0.9320	94.18%	0.9259	95.01%	0.9362
1999	94.09%	0.9248	94.96%	0.9359	94.43%	0.9290
2001	93.43%	0.9165	97.61%	0.9698	91.49%	0.8919
2004	98.21%	0.9769	98.37%	0.979	96.42%	0.9537
2008	92.64%	0.9057	93.13%	0.912	92.80%	0.9082
2010	94.53%	0.9289	92.87%	0.9082	91.54%	0.8901
2014	95.16%	0.9361	95.76%	0.9445	93.80%	0.9183
2016	91.82%	0.8957	89.20%	0.8638	92.64%	0.9062
2020	95.88%	0.9475	90.72%	0.8811	90.72%	0.8822
2022	86.76%	0.8285	76.91%	0.7056	90.88%	0.8822
Mean	93.26%	0.9130	92.38%	0.9024	92.80%	0.9074

3.2. Spatio-Temporal Changes in Wetland Landscape

The Dongting Lake wetland landscape exhibited distinct spatial distribution characteristics, with water, mudflat, reed, and sedge forming dominant patterns. Water and mudflat constituted the corridor, while woodland was mainly distributed in stripes or patches sporadically in the West and South Dongting Lake, as shown in Figure 3.

The area of water and mudflat averaged 1094.92 km² over the years, undergoing three distinct stages of change: a gradual decrease from 1217.08 km² in 1991 to 1186.47 km² in 2001, followed by a sharp decrease to 933.80 km² from 2001 to 2014 and then a steady increase to 1117.24 km² from 2014 to 2022 (Figure 4). The rapid declines of 9.12% and 5.64% annually from 2001 to 2004 may be attributed to the establishment of the Three Gorges Dam (Table 3). The average vegetation area was 1837.88 km², primarily comprising sedge, reed, and woodland, accounting for approximately 22.63%, 28.41%, and 5.40% of the Dongting Lake wetland area, respectively. Reed area exhibited an increasing trend from 926.50 km² in 1991 to 1285.18 km² in 2010, followed by a gradual decrease to 854.54 km². Notably, the annual growth rate from 2001 to 2010 (19.38 km²/a) surpassed that of 1991–2001 (18.41 km²/a). Conversely, the sedge area decreased from 629.60 km² to 589.42 km² initially due to reed expansion but later slowly rebounded to 773.95 km² as the reed area reduced. Woodland area fluctuated from 159.63 km² in 1991 to 334.01 km² in 2016, especially rising by 136.57% between 2001 and 2004. However, it dropped to 149.64 km² in 2022, marking a rapid 6.43% decline. The comprehensive dynamic degree model showed the most significant landscape dynamics from 2001 to 2004, measured at 4.03%, surpassing those of 1991–2001 and 2004–2022. This period witnessed the most pronounced landscape changes,

attributed primarily to the establishment of the Three Gorges Dam, which significantly influenced the distribution pattern of Dongting Lake wetland.

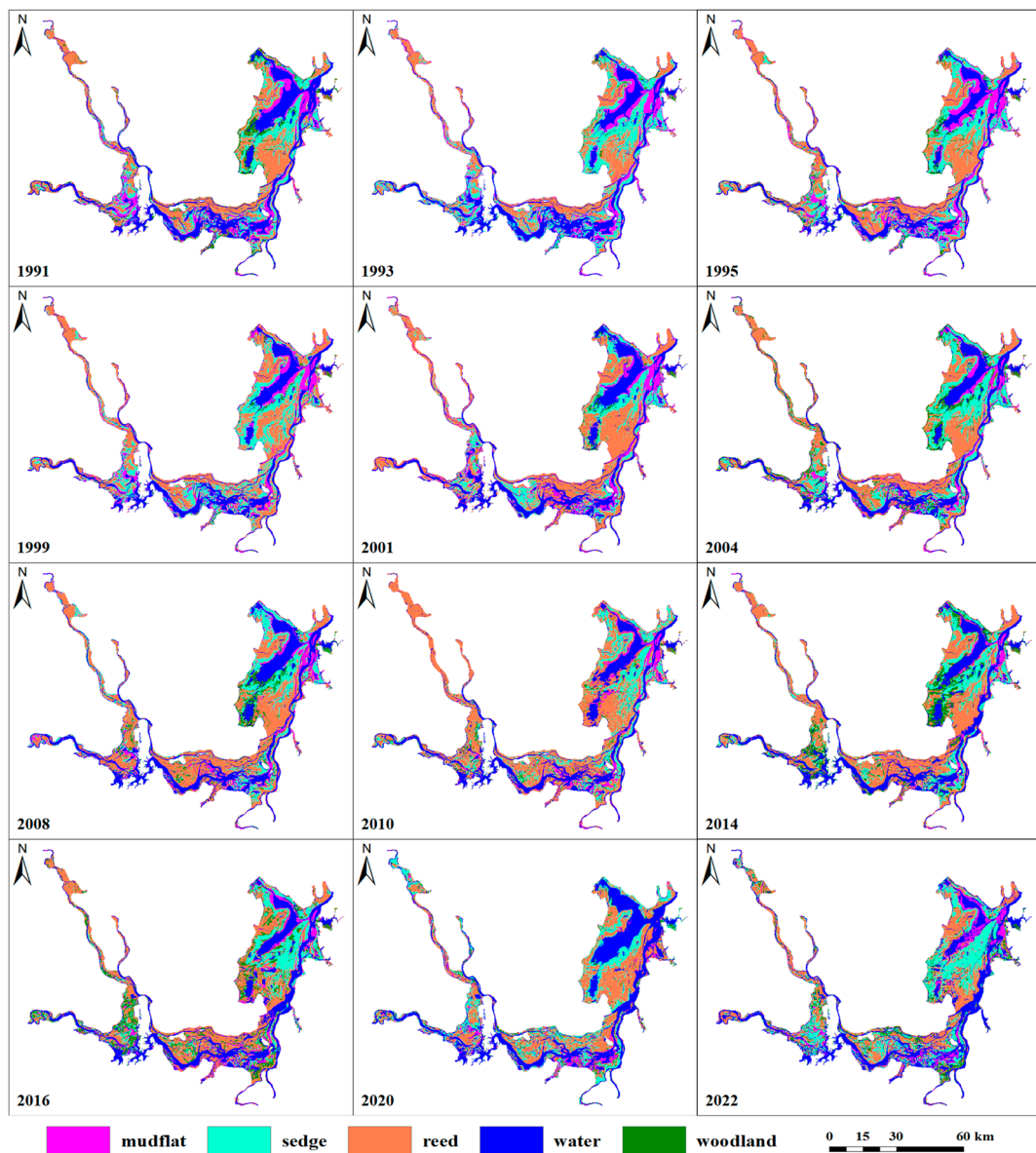


Figure 3. Landscape pattern of Dongting Lake wetland from 1991 to 2022.

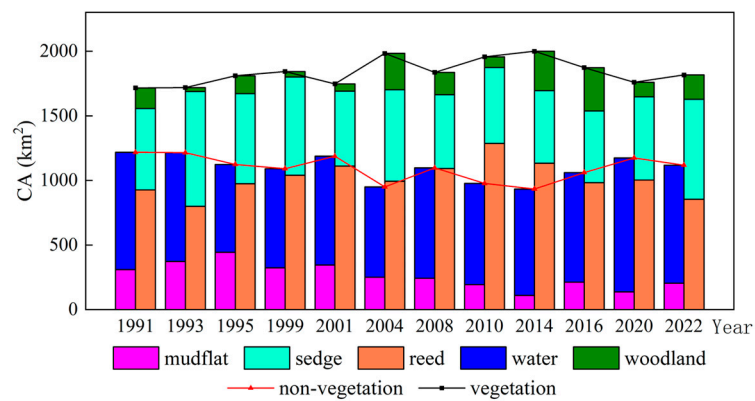


Figure 4. Change trend of landscape area in Dongting Lake wetland from 1991 to 2022.

Table 3. Landscape dynamics degree of Dongting Lake wetland from 1991 to 2022.

Time Interval	Mudflat	Water	Reed	Sedge	Woodland	Total
1991–2001	1.12%	−0.72%	1.99%	−0.78%	−6.55%	0.75%
2001–2004	−9.12%	−5.64%	−3.54%	7.40%	136.57%	4.03%
2004–2022	−1.04%	1.70%	−0.77%	0.50%	−1.85%	0.53%

Figure 5, combined with the transition matrix (Table S1), showed that the mutual conversion of vegetation, particularly between sedge and reed, emerged as a predominant trend in landscape pattern change in Dongting Lake wetland from 1991 to 2022. Specifically, within different time periods, a considerable portion of sedge area transitioned into reed area annually, with percentages of 48.83%, 28.33%, and 21.72%, while reed area transitioned into sedge area at rates of 20.91%, 23.54%, and 19.87%. The conversion of woodland areas was also significant. Before and after the construction of the Three Gorges Dam, there was a predominant outflow of woodland area (net outflow of 104.70 km² and 93.42 km²), mainly converting into reed and sedge. During the construction period, there was a predominant inflow (net inflow of 225.54 km²), with other landscape types converting into woodland in different degrees. In addition, the construction of the Three Gorges Dam directly affected the conversion of water and mudflat. Before its completion (1991–2004), the reduced area of water (195.05 km², 200.28 km²) was greater than the increased area (129.77 km², 57.96 km²). Especially during the construction period, the area of water and mudflat decreased sharply, with about 11% of water converted into mudflat, 13% converted into vegetation, and about 48% of mudflat converted into vegetation. Subsequently (2004–2022), the increase in water area (841.68 km²) outweighed the decrease (699.33 km²) due to water storage; vegetation was again submerged, and the water area gradually recovered.

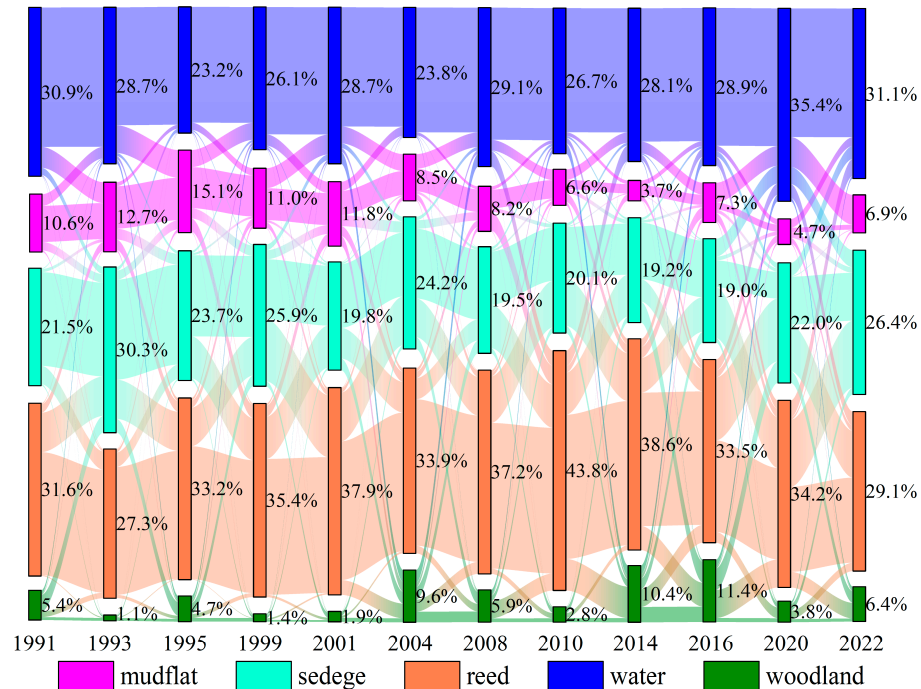


Figure 5. Transition diagram of Dongting Lake wetland landscape area from 1991 to 2022.

Through the Dongting Lake wetland landscape pattern index (Figure 6), it can be seen that (1) The degree of landscape fragmentation increased. PD and ED from 1991 and 2022 increased from 6.85 and 48.42 in 1991 to 9.92 and 61.68 in 2022, respectively, indicating that the landscape types were constantly being divided by boundaries, resulting in increased landscape fragmentation and deepening crisscrossing of landscape types.

(2) The heterogeneity of the landscape decreased. Over the years, the average SHDI and SHEI values were 1.41 and 0.876, respectively, showing a slight downward trend with fluctuations. The landscape was dominated by one or a few patch types, leading to reduced diversity and increased stability. (3) The shape of the landscape became more complex. The average FRAC_MN value remained relatively stable at 1.055, while LSI exhibited a gradual increasing trend, rising from 72.93 in 1991 to a maximum of 90.87 in 2022, with the lowest being 69.22 in 2014. This reflected an increase in the irregularity of the landscape type shape, with scattered patches and a progressively diversified landscape shape.

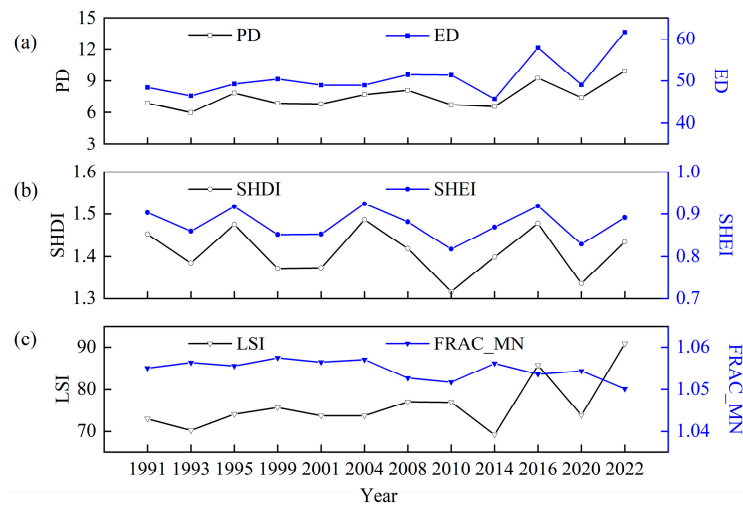


Figure 6. (a) Landscape fragmentation indices, (b) landscape diversity indices, and (c) landscape heterogeneity indices change in Dongting Lake wetland from 1991 to 2022.

3.3. Driving Factors of Wetland Landscape

The degradation of Dongting Lake was primarily attributed to the changing climate, sedimentation, and hydraulic engineering construction [37]. Due to many factors potentially affecting wetland change, the dominant factor was still debatable. In this study, natural factors (T , P , ET_p) and social factors (H) were utilized to assess the driving forces of Dongting Lake wetland change from 1991 to 2022.

The combined effects of T , P , H , and ET_p jointly affected landscape pattern index change. Nevertheless, analyzing extreme values of each factor revealed that no single factor strictly corresponded to changes in wetland landscape area and landscape pattern index. Over the years, the average winter T , P , and ET_p were 9.7°C , 34.29 mm , and 50.19 mm , respectively (Figure 7). The minimum P occurred in 1999 (0.57 mm), and the maximum occurred in 2001 (90.10 mm). Similarly, the minimum ET_p was 38.94 mm in 2016, and the maximum was 63.69 mm in 2010. Moreover, there was an extreme drought in 2022 characterized by low winter P , high ET_p , and low T ; H of Chenglingji Hydrological Station had reached a new historical low, and the landscape pattern index had significant changes compared to previous years.

RDA, a multivariate statistical method combining multiple regression and principal component analysis, was primarily employed to explore the relationship between multivariate response data and explanatory variables. In the RDA result (Figure 8a), the angle between the landscape pattern index and four factors revealed that P was almost positively correlated with the landscape index, while T , H , and ET_p were generally negatively correlated. The length of the arrow indicated that H and ET_p had the most substantial impact on landscape change as they exhibited the longest projection length on landscape area and index.

GRA, a quantitative method for measuring the degree of correlation between different factors, was used to analyze dynamic development quantitatively. In the GRA result (Figure 8b), the importance ranking of the four factors affecting landscape change was $H > ET_p > P > T$. Both analysis methods indicated that H and ET_p were critical factors.

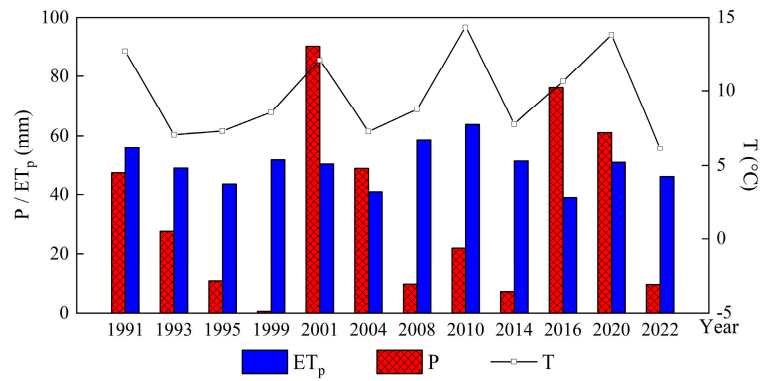


Figure 7. Trends in temperature, precipitation, and potential evaporation in Dongting Lake wetland during winter (October–December) from 1991 to 2022.

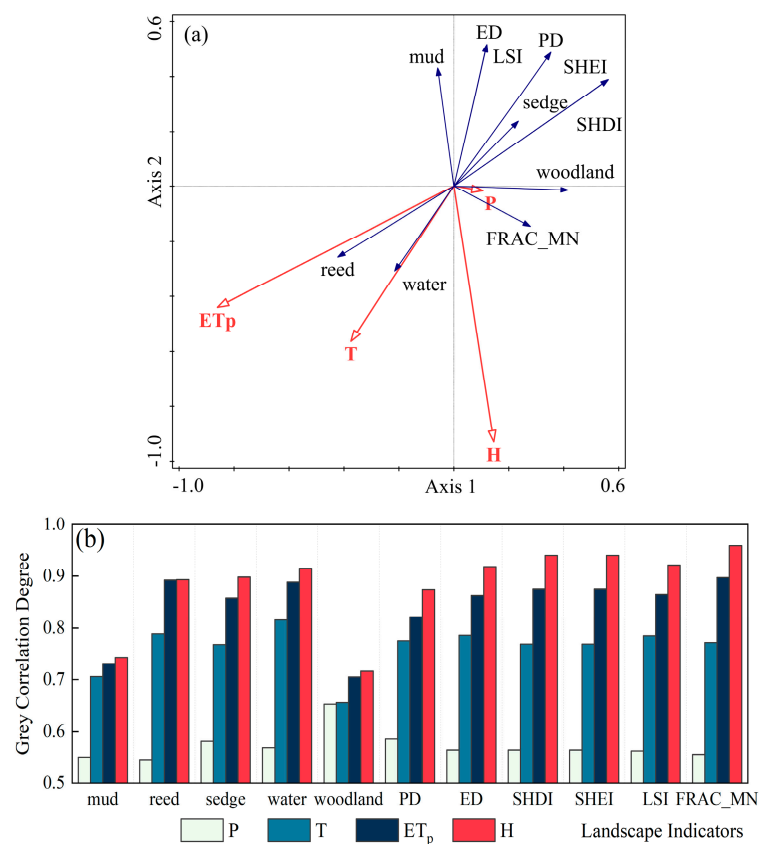


Figure 8. (a) RDA and (b) GRA results of the wetland landscape pattern index and driving factors in Dongting Lake wetland from 1991 to 2022 (the wetland landscape area and index are represented by black solid arrows, while natural and socio-economic factors are represented by red hollow arrows in RDA results).

4. Discussion

4.1. Influencing Forces of Dongting Lake Wetland Dynamics

It is commonly accepted that the combined effect of climate change (i.e., temperature, precipitation) and socio-economic activities (policy, urban expansion) is an important factor in the wetland dynamics change [38,39].

RDA analysis was also employed to assess the impact of the Three Gorges Dam on the landscape dynamics of Dongting Lake wetland pre- and post-construction (Figure 9). It was found that the explanatory rates for the first axis were 88.56% and 52.44%, respectively. During 1991–2001, T showed a slight positive correlation with the landscape index, while

P, ET_p , and H were predominantly negatively correlated. Conversely, from 2004 to 2022, P displayed a weak positive correlation with the landscape index, while T, ET_p , and H were mainly negatively correlated. The establishment of the Three Gorges Dam altered the impact mechanism of factors like water level and climate on the wetland landscape change. Furthermore, additional factors strongly intervened in landscape dynamics post-dam construction. The overall driving mechanism remained consistent with the impact mechanism after the establishment of the Three Gorges Dam (Figures 8a and 9), implying a substantial influence of the Dam on the overall landscape change trend, altering its main trajectory and evolution pattern. These findings were further supported by other studies [25,40,41]. But Wang et al. [40] also noted that a simple linear relationship between water level change and all environmental factors was not always present.

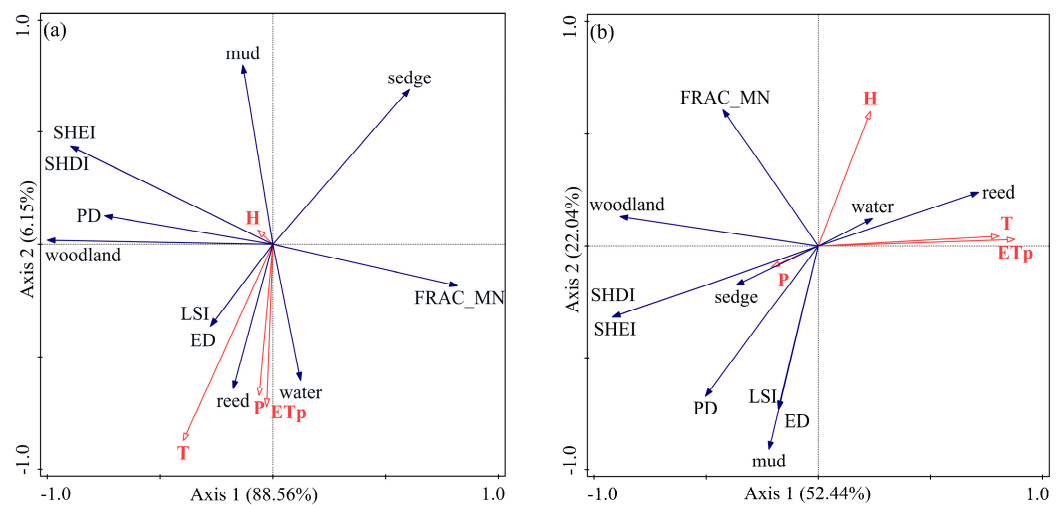


Figure 9. RDA results of the landscape pattern index and driving factors of Dongting Lake wetland (a) 1991–2001 and (b) 2004–2022.

Numerous studies have highlighted the significant impact of the water conditions on vegetation in the Dongting Lake area. Wood and reed communities were more suitable for regions with low inundation frequency, whereas grass and lake-grass communities were more adaptable to areas of high inundation frequency, suggesting that the hydrological regime determines wetland vegetation distribution [42]. Following the construction of the Three Gorges Dam, a reduction in water inflow and increased flow velocity from riverbed erosion led to significant changes in hydrological conditions and an expansion of vegetation in East Dongting Lake [43].

Due to the economic value of the reed, Large-scale artificial reed planting emerged around 2000 [44]. Forestation was the principal driving force promoting the continuous increase in Dongting Lake wetland, and returning agricultural land to wetland was also related to wetland change [45]. These factors aptly explained the observed increase in reed and woodland areas and subsequent landscape changes in Section 3.2. Long et al. [46] proposed that from 1995 to 2020, the main factors affecting wetland distribution were population density, GDP, elevation, and sunshine duration. Zhang et al. [47] highlighted solar radiation as the most significant climate factor impacting vegetation change from 2000 to 2019, surpassing the influence of temperature and precipitation. On the contrary, our study has identified water level and potential evaporation as crucial drivers of landscape patterns. Discrepancies in the selection of specific conditions and impact indicators within the study area may account for variations.

Reservoir construction, reed planting, forestation, returning farmland to lakes, and meteorological fluctuations from 1991 to 2022 collectively interacted as influencing forces in the evolution process of Dongting Lake wetland, forming a complex system (Figure 10).

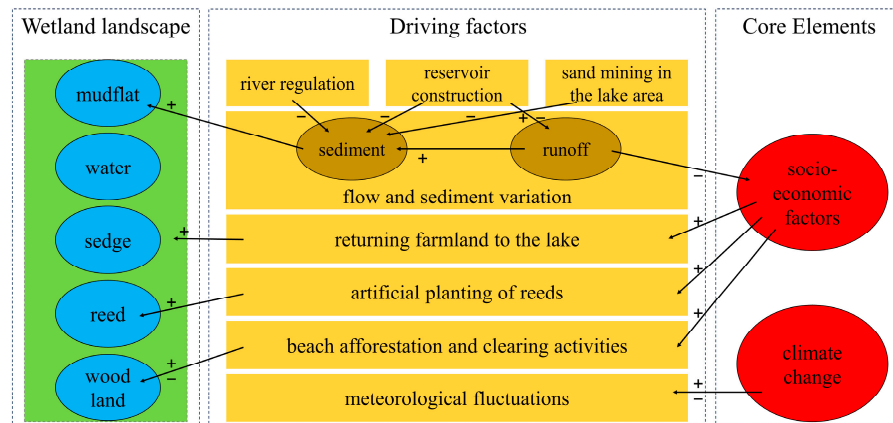


Figure 10. Influencing factors and interactions of Dongting Lake wetland evolution process from 1991 to 2022 (+ represents positive effect, and – represents negative effect).

4.2. Dynamic Evolution of Dongting Lake Wetland

Based on the spatio-temporal dynamics in Section 3.2 and the influencing forces in Section 4.1, the dynamic evolution of Dongting Lake wetland can be divided into three parts (Figure 11). (1) From 1991 to 2001, the presence of reclaimed land facilitated sediment accumulation, and the introduction of reed and poplar drove the dominant landscape transition from water to mudflat and from sedge to reed and woodland. (2) From 2001 to 2004, the impoundment of the Three Gorges Reservoir led to a reduction in the water area, prompting a transition from water to mudflat and vegetation and from sedge to reed and woodland. (3) From 2004 to 2022, partial resolution of challenges related to poplar and reed, alongside the impact of extreme drought climate events, further transformed the landscape, transitioning from mudflat and vegetation back to water and from reed and woodland to sedge.

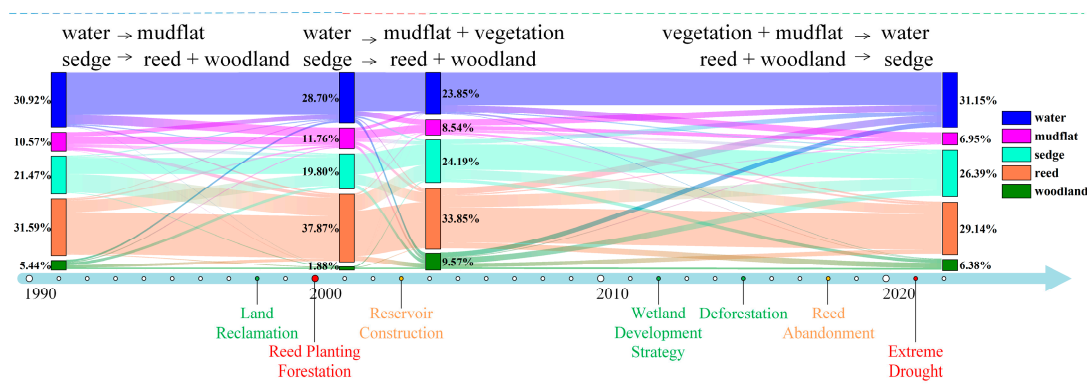


Figure 11. Driving process of wetland evolution in Dongting Lake from 1991 to 2022.

From 2000 to 2020, Dongting Lake experienced a decline in water levels during the dry season, leading to a significant reduction in wetland water area [48–50]. However, our study, which primarily focused on the dry season, revealed discrepancies compared to previous research. Specifically, from 2001 to 2004, the establishment of the Three Gorges Dam caused a decrease in the lake area, and from 2020 to 2022, the lake area decreased under extreme drought conditions despite an overall increasing trend in the water area. These inconsistencies in the evolution trend of Dongting Lake among studies can be attributed to variations in data or methodologies used and inconsistencies in defining lake boundaries. Referring to the study by Luo et al. [51] and the observed changes in the water area from 2020 to 2022, we predicted a continued decrease in the lake area.

Guo et al. [49] noted an increase in the reed area and a decrease in sedge during the dry season from 2001 to 2020. Long et al. [46] also found obvious spatial dynamics of reeds

during 2010–2020, indicating large-scale and frequent spatial transfers. While our findings aligned with previous research, we identified a new trend since 2020, characterized by a reduction in the reed and woodland area and an increase in the sedge area. Most of the literature only covers trends up to 2020, and with limited research on post-2020 trend changes, our study can provide new data support.

Furthermore, studies by Cai et al. [52] and Wu et al. [39] reported a decrease in NDVI and woodland area in West Dongting Lake due to government policies and economic profits. However, our findings suggested a sudden change in the woodland area around 2016, consistent with previous research by Zhou et al. [28] and Yu et al. [21]. Additionally, Luo et al. [51] highlighted the regional disparities in the blue–green spatial pattern index in South Dongting Lake. These studies underscore the complexity of landscape changes in Dongting Lake wetland and the heterogeneity of individual components relative to overall landscape changes.

4.3. Limitations and Future Work

In this study, Landsat images with 30 m resolution were selected, which has higher spatial resolution compared to MODIS, to explore the accuracy of three common classification methods (SVM, ML, CART) in Dongting Lake wetland. Recent studies have demonstrated that integrating MODIS/Gaofen-1/Sentinel-2/SAR and Landsat images through data fusion can provide optimal optical images for the key time periods [39,53,54]. In the subsequent work, we can employ this technique to acquire finer data.

We extracted five landscape types: water; mudflat; sedge; reed; and woodland as the objects of study, excluding cropland [50,55]. However, our findings revealed that land reclamation also impacted wetland landscape patterns. Hence, it is essential to include cropland classification for spatial and temporal variability analysis.

In analyzing wetland driving mechanisms, this paper primarily used temperature, precipitation, potential evaporation, and water level to identify the driving forces, while wetland conservation policies and other socio-economic factors like population density and GDP have important impacts on the spatial and temporal evolution of wetlands. It is crucial to further collect relevant data on other drivers and quantitatively analyze the impact of each driver.

5. Conclusions

The annual classification accuracy of the CART decision tree method, when applied to 12 Landsat images of Dongting Lake wetland from 1991 to 2022, surpassed 90%, with an average accuracy of 92.80% and a Kappa coefficient of 0.9074, demonstrating its effectiveness in Dongting Lake wetland compared to SVM and ML methods.

The water and mudflat area experienced three distinct stages of fluctuation: a gradual decrease until 2001, followed by a sharp decline until 2014, and then a steady increase. Vegetation conversion, particularly between sedge and reed, emerged as a dominant trend. Reed area initially increased, then gradually decreased, while sedge area decreased due to reed expansion but later rebounded. Woodland area fluctuated, peaking in 2016 after a rapid rise between 2001 and 2004 but declining by 2022. Throughout the years, landscape fragmentation increased, landscape heterogeneity slightly decreased, and the landscape shape became more complex with scattered patches and diversified forms.

The evolution of Dongting Lake wetland was influenced by both natural factors such as temperature, precipitation, evapotranspiration, and eco-social factors, including reservoir construction, reed and polar planting, and farmland reclamation. The construction of the Three Gorges Dam significantly altered landscape dynamics by affecting water levels. Additionally, potential evaporation emerged as a significant natural factor impacting landscape dynamics, exhibiting a negative correlation with the landscape dynamics index.

Supplementary Materials: The following supporting information can be downloaded at: <https://www.mdpi.com/article/10.3390/w16091273/s1>, Table S1: Transition matrix of Dongting Lake wetland landscape area from 1991 to 2022 (km²).

Author Contributions: Conceptualization, N.Z. and M.G.; methodology, Y.C. and M.G.; validation, S.L.; formal analysis, S.L. and K.L.; investigation, S.L., W.Z. and K.L.; resources, W.Z.; writing—original draft preparation, M.G.; writing—review and editing, N.Z.; visualization, M.G. and K.L.; supervision, Y.C.; funding acquisition, N.Z. All authors have read and agreed to the published version of the manuscript.

Funding: This research was funded by the Strategic Research Program of the National Natural Science Foundation of China (Grant No. 42242202) and the National Natural Science Foundation of China (Grant No. 42272291).

Data Availability Statement: The datasets generated during and/or analyzed during the current study can be made available upon request.

Acknowledgments: The research team acknowledges the data support from the “National Earth System Science Data Center, National Science and Technology Infrastructure of China. (<http://www.geodata.cn>, accessed on 15 July 2023)”.

Conflicts of Interest: The authors declare no conflicts of interest.

References

- Hu, S.; Niu, Z.; Chen, Y.; Li, L.; Zhang, H. Global wetlands: Potential distribution, wetland loss, and status. *Sci. Total Environ.* **2017**, *586*, 319–327. [[CrossRef](#)] [[PubMed](#)]
- Kaplan, G.; Avdan, U. Mapping and monitoring wetlands using Sentinel-2 satellite imagery. *ISPRS Ann. Photogramm. Remote Sens. Spat. Inf. Sci.* **2017**, *4*, 271–277. [[CrossRef](#)]
- Wei, X.; Wang, S.; Wang, Y. Spatial and temporal change of fractional vegetation cover in North-western China from 2000 to 2010. *Geol. J.* **2018**, *53*, 427–434. [[CrossRef](#)]
- Shen, G.; Yang, X.; Jin, Y.; Xu, B.; Zhou, Q. Remote sensing and evaluation of the wetland ecological degradation process of the Zoige Plateau Wetland in China. *Ecol. Indic.* **2019**, *104*, 48–58. [[CrossRef](#)]
- Granata, F.; Gargano, R.; de Marinis, G. Artificial intelligence based approaches to evaluate actual evapotranspiration in wetlands. *Sci. Total Environ.* **2020**, *703*, 135653. [[CrossRef](#)] [[PubMed](#)]
- Mao, D.; Wang, Z.; Wu, J.; Wu, B.; Zeng, Y.; Song, K.; Yi, K.; Luo, L. China’s wetlands loss to urban expansion. *Land Degrad. Dev.* **2018**, *29*, 2644–2657. [[CrossRef](#)]
- Bian, H.; Li, W.; Li, Y.; Ren, B.; Niu, Y.; Zeng, Z. Driving forces of changes in China’s wetland area from the first (1999–2001) to second (2009–2011) National Inventory of Wetland Resources. *Glob. Ecol. Conserv.* **2020**, *21*, e00867. [[CrossRef](#)]
- Niu, Z.; Zhang, H.; Wang, X.; Yao, W.; Zhou, D.; Zhao, K.; Zhao, H.; Li, N.; Huang, H.; Li, C. Mapping wetland changes in China between 1978 and 2008. *Chin. Sci. Bull.* **2012**, *57*, 2813–2823. [[CrossRef](#)]
- Bansal, S.; Creed, I.F.; Tangen, B.A.; Bridgham, S.D.; Desai, A.R.; Krauss, K.W.; Neubauer, S.C.; Noe, G.B.; Rosenberry, D.O.; Trettin, C.; et al. Practical Guide to Measuring Wetland Carbon Pools and Fluxes. *Wetlands* **2023**, *43*, 105. [[PubMed](#)]
- Zhao, C.; Gong, J.; Zeng, Q.; Yang, M.; Wang, Y. Landscape pattern evolution processes and the driving forces in the wetlands of lake Baiyangdian. *Sustainability* **2021**, *13*, 9747. [[CrossRef](#)]
- Liu, Y.; Yang, P.; Zhang, S.; Wang, W. Dynamic identification and health assessment of wetlands in the middle reaches of the Yangtze River basin under changing environment. *J. Clean. Prod.* **2022**, *345*, 131105. [[CrossRef](#)]
- Yang, R.; Chen, Y.; Qiu, Y.; Lu, K.; Wang, X.; Sun, G.; Liang, Q.; Song, H.; Liu, S. Assessing the Landscape Ecological Health (LEH) of Wetlands: Research Content and Evaluation Methods (2000–2022). *Water* **2023**, *15*, 2410. [[CrossRef](#)]
- Melnychenko, T.; Solovey, T. Mapping Water Bodies and Wetlands from Multispectral and SAR Data for the Cross-Border River Basins of the Polish–Ukrainian Border. *Water* **2024**, *16*, 407. [[CrossRef](#)]
- Shi, K.; Zhang, Y.; Zhu, G.; Liu, X.; Zhou, Y.; Xu, H.; Qin, B.; Liu, G.; Li, Y. Long-term remote monitoring of total suspended matter concentration in Lake Taihu using 250 m MODIS-Aqua data. *Remote Sens. Environ.* **2015**, *164*, 43–56. [[CrossRef](#)]
- Ahmadzadeh, R.; Dehdar, D.M.; Khorasani, N.; Farsad, F.; Rahimibashar, M.R. Assessment of wetland landscape changes based on landscape metrics and trophic state index (case study: Anzali International Wetland). *Environ. Monit. Assess.* **2023**, *195*, 1206. [[CrossRef](#)] [[PubMed](#)]
- Fan, C.; Yang, J.; Zhao, G.; Dai, J.; Zhu, M.; Dong, J.; Liu, R.; Zhang, G. Mapping Phenology of Complicated Wetland Landscapes through Harmonizing Landsat and Sentinel-2 Imagery. *Remote Sens.* **2023**, *15*, 2413. [[CrossRef](#)]
- Zhang, M.; Lin, H. Wetland classification using parcel-level ensemble algorithm based on Gaofen-6 multispectral imagery and Sentinel-1 dataset. *J. Hydrol.* **2022**, *606*, 127462. [[CrossRef](#)]

18. Cheng, S.; Yang, X.; Yang, G.; Chen, B.; Chen, B.; Wang, J.; Ren, K.; Sun, W. Using ZY1-02D satellite hyperspectral remote sensing to monitor landscape diversity and its spatial scaling change in the Yellow River Estuary. *Int. J. Appl. Earth Obs. Geoinf.* **2024**, *128*, 103716. [[CrossRef](#)]
19. Wang, J.; Sheng, Y.; Tong, T.S.D. Monitoring decadal lake dynamics across the Yangtze Basin downstream of Three Gorges Dam. *Remote Sens. Environ.* **2014**, *152*, 251–269. [[CrossRef](#)]
20. Lamsal, P.; Atreya, K.; Ghosh, M.K.; Pant, K.P. Effects of population, land cover change, and climatic variability on wetland resource degradation in a Ramsar listed Ghodaghodi Lake Complex, Nepal. *Environ. Monit. Assess.* **2019**, *191*, 415. [[CrossRef](#)]
21. Yu, S.; Li, C.a.; Yu, D.; He, Q.; Luo, W.; Xiang, F. Land Cover Change on Beach of Dongting Lake's Beach. *J. Earth Sci.* **2020**, *45*, 1918–1927.
22. Peng, Y.; He, G.; Wang, G.; Cao, H. Surface Water Changes in Dongting Lake from 1975 to 2019 Based on Multisource Remote-Sensing Images. *Remote Sens.* **2021**, *13*, 1827. [[CrossRef](#)]
23. Ye, W. Remote sensing image land type data mining based on QUEST decision tree. *Clust. Comput.* **2019**, *22*, 8437–8443.
24. Hu, J.; Xie, Y.; Tang, Y.; Li, F.; Zou, Y. Changes of Vegetation Distribution in the East Dongting Lake After the Operation of the Three Gorges Dam, China. *Front. Plant Sci.* **2018**, *9*, 582. [[CrossRef](#)]
25. Hu, Y.; Huang, J.; Du, Y.; Han, P.; Wang, J.; Huang, W. Monitoring wetland vegetation pattern response to water-level change resulting from the Three Gorges Project in the two largest freshwater lakes of China. *Ecol. Eng.* **2015**, *74*, 274–285. [[CrossRef](#)]
26. Lai, X.; Jiang, J.; Huang, Q. Effects of the normal operation of the Three Gorges Reservoir on wetland inundation in Dongting Lake, China: A modelling study. *Hydrol. Sci. J.* **2013**, *58*, 1467–1477. [[CrossRef](#)]
27. Yang, L.; Wang, L.; Yu, D.; Yao, R.; He, Q.; Wang, S.; Wang, L. Four decades of wetland changes in Dongting Lake using Landsat observations during 1978–2018. *J. Hydrol.* **2020**, *587*, 124954. [[CrossRef](#)]
28. Zhou, J.; Wan, R.; Wu, X.; Zhang, Y. Patterns of long-term distribution of typical wetland vegetation (1987–2016) and its response to hydrological processes in Lake Dongting. *J. Lake Sci.* **2020**, *32*, 1723–1735.
29. Chen, J.; Zhu, X.; Vogelman, J.E.; Gao, F.; Jin, S. A simple and effective method for filling gaps in Landsat ETM + SLC-off images. *Remote Sens. Environ.* **2011**, *115*, 1053–1064. [[CrossRef](#)]
30. Penman, H.L. Natural evaporation from open water, bare soil and grass. *Proc. R. Soc. Lond. Ser. A-Math. Phys. Eng. Sci.* **1948**, *193*, 120–145.
31. Chi, D.; Wang, H.; Li, X.; Liu, H.; Li, X. Estimation of the ecological water requirement for natural vegetation in the Ergune River basin in Northeastern China from 2001 to 2014. *Ecol. Indic.* **2018**, *92*, 141–150. [[CrossRef](#)]
32. Masurkar, A.; Daruwala, R.; Mohite, A. Performance analysis of SAR filtering techniques using SVM and Wishart Classifier. *Remote Sens. Appl.-Soc. Environ.* **2024**, *34*, 101189. [[CrossRef](#)]
33. Rimal, B.; Rijal, S.; Kunwar, R. Comparing Support Vector Machines and Maximum Likelihood Classifiers for Mapping of Urbanization. *J. Indian Soc. Remote Sens.* **2020**, *48*, 71–79. [[CrossRef](#)]
34. Lin, W.; Cen, J.; Xu, D.; Du, S.; Gao, J. Wetland landscape pattern changes over a period of rapid development (1985–2015) in the ZhouShan Islands of Zhejiang province, China. *Estuar. Coast. Shelf Sci.* **2018**, *213*, 148–159. [[CrossRef](#)]
35. Yao, B.; Zhang, H.; Liu, Y.; Liu, H.; Ling, C. Remote Sensing Classification of Wetlands based on Object-oriented and CART Decision Tree Method. *For. Res.* **2019**, *32*, 91–98.
36. Tardanico, J.; Hovestadt, T. Effects of compositional heterogeneity and spatial autocorrelation on richness and diversity in simulated landscapes. *Ecol. Evol.* **2023**, *13*, e10810. [[CrossRef](#)] [[PubMed](#)]
37. Xie, C.; Huang, X.; Mu, H.; Yin, W. Impacts of Land-Use Changes on the Lakes across the Yangtze Floodplain in China. *Environ. Sci. Technol.* **2017**, *51*, 3669–3677. [[CrossRef](#)]
38. Liu, J.; Gao, J.; Dong, C. Regional differentiation and factors influencing changes in swamps in the Sanjiang Plain from 1954 to 2015. *Acta Ecol. Sin.* **2019**, *39*, 4821–4831.
39. Wu, L.; Li, Z.; Liu, X.; Zhu, L.; Tang, Y.; Zhang, B.; Xu, B.; Liu, M.; Meng, Y.; Liu, B. Multi-Type Forest Change Detection Using BFAST and Monthly Landsat Time Series for Monitoring Spatiotemporal Dynamics of Forests in Subtropical Wetland. *Remote Sens.* **2020**, *12*, 341. [[CrossRef](#)]
40. Wang, H.; Bai, X.; Huang, L.; Hong, F.; Yuan, W.; Guo, W. The spatial variation of hydrological conditions and their impact on wetland vegetation in connected floodplain wetlands: Dongting Lake Basin. *Environ. Sci. Pollut. Res. Int.* **2024**, *31*, 8483–8498. [[CrossRef](#)]
41. Huang, Y.; Chen, X.; Li, F.; Hou, Z.; Li, X.; Zeng, J.; Deng, Z.; Zou, Y.; Xie, Y. Community Trait Responses of Three Dominant Macrophytes to Variations in Flooding During 2011–2019 in a Yangtze River-Connected Floodplain Wetland (Dongting Lake, China). *Front. Plant Sci.* **2021**, *12*, 604677. [[CrossRef](#)]
42. Deng, F.; Wang, X.; Cai, X.; Li, E.; Jiang, L.; Li, H.; Yan, R. Analysis of the relationship between inundation frequency and wetland vegetation in Dongting Lake using remote sensing data. *Ecology* **2014**, *7*, 717–726. [[CrossRef](#)]
43. Xie, Y.; Tang, Y.; Chen, X.; Li, F.; Deng, Z. The impact of Three Gorges Dam on the downstream eco-hydrological environment and vegetation distribution of East Dongting Lake. *Ecology* **2015**, *8*, 738–746. [[CrossRef](#)]
44. Zhang, Y.; Wang, D.; Wu, X.; Lai, X. Driving factors of wetland evolution in Lake Dongting during 1900–2020. *J. Lake Sci.* **2023**, *35*, 1786–1795.
45. Yang, Z.; Han, L.; Liu, Q.; Li, C.; Pan, Z.; Xu, K. Spatial and Temporal Changes in Wetland in Dongting Lake Basin of China under Long Time Series from 1990 to 2020. *Sustainability* **2022**, *14*, 3620. [[CrossRef](#)]

46. Long, X.; Lin, H.; An, X.; Chen, S.; Qi, S.; Zhang, M. Evaluation and analysis of ecosystem service value based on land use/cover change in Dongting Lake wetland. *Ecol. Indic.* **2022**, *136*, 108619. [[CrossRef](#)]
47. Zhang, M.; Lin, H.; Long, X.; Cai, Y. Analyzing the spatiotemporal pattern and driving factors of wetland vegetation changes using 2000-2019 time-series Landsat data. *Sci. Total Environ.* **2021**, *780*, 146615. [[CrossRef](#)]
48. Tan, Z.; Zhang, Q.; Li, M.; Li, Y.; Xu, X.; Jiang, J. A study of the relationship between wetland vegetation communities and water regimes using a combined remote sensing and hydraulic modeling approach. *Hydrol. Res.* **2016**, *47*, 278–292.
49. Guo, D.; Shi, W.; Qian, F.; Wang, S.; Cai, C. Monitoring the spatiotemporal change of Dongting Lake wetland by integrating Landsat and MODIS images, from 2001 to 2020. *Ecol. Inf.* **2022**, *72*, 101848. [[CrossRef](#)]
50. Peng, H.; Xia, H.; Shi, Q.; Tang, Z.; Chen, H. Monitoring of wetland cover changes in protected areas to trade-offs between ecological conservation and food security: A case study from the Dongting Lake, China. *Ecol. Inf.* **2023**, *78*, 102338. [[CrossRef](#)]
51. Luo, Q.; Li, Y.; Cao, X.; Jiang, S.; Yu, H. The Spatial and Temporal Variability of the Blue–Green Spatial Structures of the South Dongting Lake Wetland Areas Amidst Climate Change, including Its Relationship with Meteorological Factors. *Water* **2024**, *16*, 209. [[CrossRef](#)]
52. Cai, Y.; Liu, S.; Lin, H. Monitoring the Vegetation Dynamics in the Dongting Lake Wetland from 2000 to 2019 Using the BEAST Algorithm Based on Dense Landsat Time Series. *Appl. Sci.* **2020**, *10*, 4209. [[CrossRef](#)]
53. Song, R.; Lin, H.; Wang, G.; Yan, E.; Ye, Z. Improving Selection of Spectral Variables for Vegetation Classification of East Dongting Lake, China, Using a Gaofen-1 Image. *Remote Sens.* **2018**, *10*, 50. [[CrossRef](#)]
54. Xing, L.; Tang, X.; Wang, H.; Fan, W.; Gao, X. Mapping Wetlands of Dongting Lake in China Using Landsat and sentinel-1 time series at 30M. *Int. Arch. Photogramm. Remote Sens. Spat. Inf. Sci.* **2018**, *42*, 1971–1976. [[CrossRef](#)]
55. Cai, Y.; Lin, H.; Zhang, M. Mapping paddy rice by the object-based random forest method using time series Sentinel-1/Sentinel-2 data. *Adv. Space Res.* **2019**, *64*, 2233–2244. [[CrossRef](#)]

Disclaimer/Publisher’s Note: The statements, opinions and data contained in all publications are solely those of the individual author(s) and contributor(s) and not of MDPI and/or the editor(s). MDPI and/or the editor(s) disclaim responsibility for any injury to people or property resulting from any ideas, methods, instructions or products referred to in the content.